

Quantum thermal machine regimes in the transverse-field Ising model

Vishnu Muraleedharan Sajitha,^{1, 2, 3,*} Bodhaditya Santra,³ Matthew J. Davis,^{2, †} and L. A. Williamson^{2, ‡}

¹University of Queensland – IIT Delhi Academy of Research (UQIDAR), Hauz Khas, New Delhi 110016, India

²ARC Centre of Excellence for Engineered Quantum Systems, School of Mathematics and Physics, University of Queensland, St Lucia, Queensland 4072, Australia

³Department of Physics, Indian Institute of Technology, Delhi, New Delhi 110016, India

(Dated: March 14, 2025)

We identify and interpret the possible quantum thermal machine regimes with a transverse-field Ising model as the working substance. In general, understanding the emergence of such regimes in a many-body quantum system is challenging due to the dependence on the many energy levels in the system. By considering infinitesimal work strokes, we can understand the operation from equilibrium properties of the system. We find that infinitesimal work strokes enable both heat engine and accelerator operation, with the output and boundaries of operation described by macroscopic properties of the system, in particular the net transverse magnetization. At low temperatures, the regimes of operation and performance can be understood from quasiparticles in the system, while at high temperatures an expansion of the free energy in powers of inverse temperature describes the operation. The understanding generalises to larger work strokes when the temperature difference between the hot and cold reservoirs is large. For hot and cold reservoirs close in temperature, a sufficiently large work stroke can enable refrigerator and heater regimes. Our results and method of analysis will prove useful in understanding the possible regimes of operation of quantum many-body thermal machines more generally.

I. INTRODUCTION

A thermal machine, such as an engine or a refrigerator, consists of a working substance that utilises the flow of heat to achieve a useful task. Quantum thermal machines incorporate quantum effects in the working substance or reservoirs, providing possible performance advantages and insights into thermodynamics at the quantum scale [1]. While this field has a long history in single-particle or non-interacting systems [2–5], recent interest has been directed toward interacting many-body quantum systems [6, 7]. Entanglement [8–10], interactions [11–19] and many-body localization [20] have been shown to enable or enhance thermodynamic tasks compared to the comparative non-interacting system.

As for a classical working substance, a quantum working substance may support different regimes of operation depending on the magnitude and duration of the work stroke and the temperature of the reservoirs [21]. However, in quantum systems, the work stroke depends on the underlying protocol, such as the two-point projective measurement scheme [22], where the control parameter in the Hamiltonian is changed from an initial value to a final value. The regimes of operation for a quantum working substance will depend on how the energies of the eigenstate change during the work stroke. Interacting quantum systems generally have a vast number of irregularly spaced energy levels. Hence, isolated work steps, even if adiabatic, can result in deviation from a thermal state due to energy levels that generally move incommen-

surately [23, 24]. Therefore, understanding the regimes of operation from simple physical properties of the system is a challenging task even under adiabatic operation.

Arrays of interacting quantum spins are an ideal system to explore quantum many-body physics due to their rich physics and high degree of experimental control [25–31], with realizations involving hundreds of spins using trapped ions [26, 29] and Rydberg atoms [30, 31]. Recently, the operation of this system as a working substance for thermodynamic tasks has become a topical area of theoretical exploration [16, 21, 32–34]. For nearest-neighbour interactions, performance enhancement and universal behaviour have been identified close to the quantum critical point [16, 33, 34]. Enhancements due to long-range interactions have also been identified [16, 35, 36].

In this paper we characterise the possible regimes of adiabatic operation of a thermal machine using a spin chain with nearest-neighbor interactions as the working substance. As in previous studies, work is done on or by the system by tuning a driving field transverse to the spin interactions. We present a novel analysis based on an infinitesimal work step, which ensures the system remains in thermal equilibrium. With infinitesimal work steps, only engine or accelerator regimes are permitted. We explain the regimes of operation and the magnitude of the work output in both the high and low temperature limits utilising a high temperature expansion and a quasiparticle approximation respectively. Boundaries between the heat engine and accelerator regimes are identified and related to the behaviour of the macroscopic magnetization of the system.

Building on the understanding provided by infinitesimal work strokes, we extend our analysis to finite-size work steps. For large differences in temperature between the cold and hot bath, the regimes of operation are qualita-

* v.muraleedharansajitha@uq.edu.au

† mdavis@uq.edu.au

‡ lewis.williamson@uq.edu.au

tively similar to the infinitesimal case, with a shift in the boundary between accelerator and heat engine that can be understood from the quasiparticle spectrum. As the difference in the temperatures of the two reservoirs becomes small, refrigerator and heater regimes can emerge, particularly close to the quantum critical point of the system.

This paper is organised as follows. In Sec. II we introduce the model, parameterise the thermodynamic cycle, and describe the possible regimes of operation. In Sec. III we present our results: we present and interpret the regimes of operation and performance of a thermal machine with an infinitesimal work stroke, and then extend this analysis to a finite-size work stroke. We conclude in Sec. IV.

II. FORMALISM

A. The transverse-field Ising model

We consider a one-dimensional working substance consisting of N spin-1/2 particles with nearest-neighbour interactions. The Hamiltonian of the system is given by the transverse-field Ising model,

$$H = -g \sum_{j=1}^{N-1} \hat{\sigma}_j^x \hat{\sigma}_{j+1}^x - h \sum_{j=1}^N \hat{\sigma}_j^z, \quad (1)$$

where $\hat{\sigma}_j^\mu$ are Pauli operators acting on the j^{th} site ($[\hat{\sigma}_j^\mu, \hat{\sigma}_j^\nu] = 2i\epsilon_{\mu\nu\kappa}\hat{\sigma}_j^\kappa$), $g > 0$ is the interaction strength and h is the transverse field strength. In the thermodynamic limit ($N \rightarrow \infty$) the transverse-field Ising model has a quantum critical point at $g = |h|$ separating the ferromagnetic ($g > |h|$) and paramagnetic ($g < |h|$) ground states [37]. Here, Eq. (1) can be diagonalised following a Jordan-Wigner transformation from spins to free fermions, which gives [38]

$$H = E_0 + \sum_{j=1}^N \omega(\theta_j) \hat{c}_j^\dagger \hat{c}_j. \quad (2)$$

Here \hat{c}_j , $j = 1, \dots, N$ are fermion annihilation operators with spectra

$$\omega(\theta_j) = 2\sqrt{h^2 + g^2 - 2gh \cos \theta_j}, \quad \theta_j = \frac{\pi(2j-1)}{N}, \quad (3)$$

and $E_0 = -\frac{1}{2} \sum_j \omega(\theta_j)$ is the ground state energy.

B. The quantum Otto cycle

Among the various possible thermodynamic cycles that can be used to realise thermal machines, we choose an Otto cycle due to the ease with which heat and work

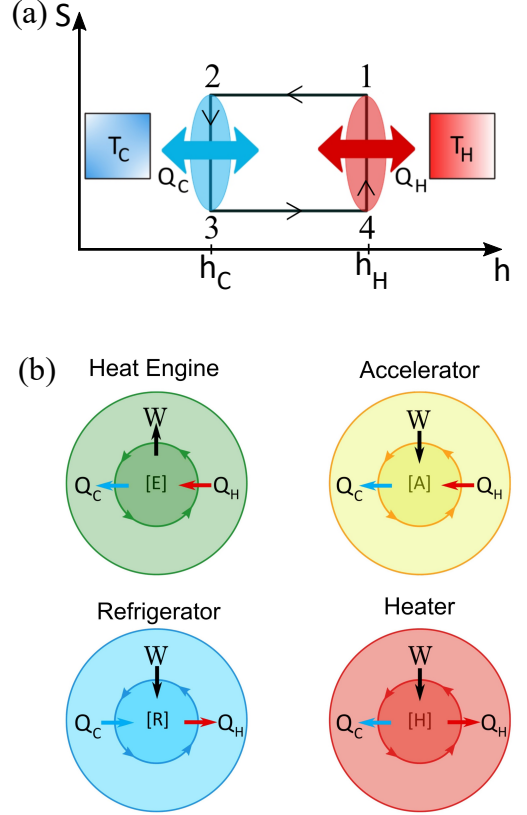


FIG. 1. (a) A schematic diagram of an Otto cycle in the $S - h$ plane, where S is the von-Neumann entropy. Work is exchanged by tuning the transverse field h during the two unitary work strokes $1 \rightarrow 2$ and $3 \rightarrow 4$. Heat is exchanged during the two thermalization strokes $4 \rightarrow 1$ and $2 \rightarrow 3$. (b) The four possible thermal machine operations, determined by the signs of work and heat flows.

can be distinguished [39, 40]. The quantum Otto cycle consists of four strokes as illustrated in Fig. 1(a) [41]. The system begins in a hot thermal state at 1. Step $(1 \rightarrow 2)$: The system is thermally isolated and the driving field h is adiabatically tuned from h_H to h_C . Work $W_{1 \rightarrow 2}$ is done by the system. Step $(2 \rightarrow 3)$: The system is coupled to the cold reservoir with h fixed, exchanging heat Q_C until thermal equilibrium is achieved at 3. Step $(3 \rightarrow 4)$: The system is thermally isolated and h is adiabatically tuned from h_C to h_H . Work $W_{3 \rightarrow 4}$ is done by the system. Step $(4 \rightarrow 1)$: The system is coupled to the hot reservoir with h fixed, exchanging heat Q_H until thermal equilibrium is achieved at 1.

The total work done in the cycle is

$$W = W_{1 \rightarrow 2} + W_{3 \rightarrow 4} = -(Q_C + Q_H). \quad (4)$$

The first and second laws of thermodynamics permit four possible regimes of thermal machines, depending on the signs of heat and work [42], see Fig. 1(b):

- Engine [E]: Utilises the thermodynamic flow of heat to do work; $W < 0, Q_H > 0, Q_C < 0$.

- Accelerator [A]: Increases the thermodynamic flow of heat using work; $W > 0, Q_H > 0, Q_C < 0$.
- Refrigerator [R]: Utilises work to reverse the thermodynamic flow of heat; $W > 0, Q_H < 0, Q_C > 0$.
- Heater [H]: Utilises work to transfer heat to both reservoirs; $W > 0, Q_H < 0, Q_C < 0$.

We use the convention that a negative value of heat or work is an output and a positive value an input. The thermodynamic flow of heat is a flow of heat from the hot to the cold reservoir.

In the thermodynamic limit the spacing between fermionic mode frequencies [Eq. (3)] becomes infinitesimal, and summations \sum_j over fermionic modes can be replaced by an integral $\frac{N}{\pi} \int_0^\pi d\theta$. Then the total adiabatic work output for the cycle in Fig. 1 is [21]

$$W = \int_0^\pi (\omega_C(\theta) - \omega_H(\theta)) (f_H(\theta) - f_C(\theta)) d\theta. \quad (5)$$

Here $f_{H,C}(\theta) \equiv [1 + e^{\omega_{H,C}(\theta)/k_B T_{H,C}}]^{-1}$ is the Fermi-Dirac distribution, which gives the occupation of the fermionic modes in thermal equilibrium.

C. Work and heat with an infinitesimal work step

In general, the thermal machine regime is determined by how energy levels respond to changes in h and the number of energy levels contributing (i.e. temperature). To simplify our initial analysis, we consider an infinitesimal work stroke $\delta h = h_H - h_C$. For $\delta h \rightarrow 0$, Eq. (5) simplifies to

$$\begin{aligned} W &= \int_0^\pi \delta h \frac{d\omega_H(\theta)}{dh} (f_H(\theta) - f_C(\theta)) d\theta, \\ &= \delta h \left(\left\langle \frac{dE}{dh} \right\rangle_{T_C} - \left\langle \frac{dE}{dh} \right\rangle_{T_H} \right). \end{aligned} \quad (6)$$

Similarly, the heat associated with the hot and cold reservoirs are,

$$\begin{aligned} Q_H &= \langle E \rangle_{T_H} - \langle E \rangle_{T_C} - \frac{\delta h}{k_B T_H} \left\langle E \frac{dE}{dh} \right\rangle_{T_H} \\ &\quad + \delta h \left(\left\langle \frac{dE}{dh} \right\rangle_{T_H} - \left\langle \frac{dE}{dh} \right\rangle_{T_C} \right), \\ Q_C &= \langle E \rangle_{T_C} - \langle E \rangle_{T_H} + \frac{\delta h}{k_B T_H} \left\langle E \frac{dE}{dh} \right\rangle_{T_H}. \end{aligned} \quad (7)$$

For $\delta h \rightarrow 0$ we have $Q_H > 0$ and $Q_C < 0$ and hence only accelerator or engine operation is possible, depending on the sign of work. We also have the relation:

$$\left\langle \frac{dE}{dh} \right\rangle_T = \frac{dF}{dh} \quad (8)$$

where $F = -k_B T \ln Z_T$ is the free energy of the system, with $Z_T = \text{Tr } e^{-H/k_B T}$ the partition function at temperature T . Here the advantage of using an infinitesimal work stroke is clear, as it allows work and heat to be computed directly from the free energy. Using Eq. (2) the free energy is then [38]

$$F = -Nk_B T \left[\ln(2) + \frac{1}{\pi} \int_0^\pi d\theta \ln \left(\cosh \left(\frac{\omega(\theta)}{2k_B T} \right) \right) \right]. \quad (9)$$

Furthermore, using the partition function, we have

$$\frac{dF}{dh} = -M(T). \quad (10)$$

Here M is the average transverse magnetization of the system (below we will also use the magnetization per particle $m = M/N$). Hence [21, 43]

$$W = \delta h (M(T_H) - M(T_C)), \quad (11)$$

i.e. the net work exchanged is directly proportional to the difference in transverse magnetization of the system at temperatures T_H and T_C .

Equation (11) takes an analogous form to the work output of an ideal gas Otto cycle, which for infinitesimal volume change δV is

$$W_{\text{ideal gas}} = \delta V (P(T_H) - P(T_C)), \quad (12)$$

with $P = -\frac{dF}{dV}$ the pressure of the system. This pressure is monotonic with temperature, resulting in operation fixed by the sign of δV . Similarly, setting $g = 0$ in Eq. (1) results in operation fixed by the sign of δh . In general, for simple non-interacting systems where all energy levels vary monotonically with the control parameter, the type of operation is fixed by the sign of the change in control parameter.

III. RESULTS

A. Thermal machine regimes for the transverse-field Ising model

The work output and regimes of operation for the Otto cycle (Fig. 1) with infinitesimal work step $\delta h > 0$ are shown in Fig. 2(a). As already noted, with infinitesimal work step only accelerator or engine regimes are possible, with the regime of operation determined by the sign of $M(T_H) - M(T_C)$ (Eq. (11)). When $M(T_H) < M(T_C)$ the system operates as an engine, whereas for $M(T_H) > M(T_C)$ the system operates as an accelerator. For $\delta h < 0$, the sign of work is reversed and the engine and accelerator regimes are switched.

Due to the connection between work and $M(T)$, the regimes of operation can be understood from the behaviour of $M(T)$. Example behaviour of $M(T)$ are illustrated in Fig. 2(b) and Fig. 3. The engine and accelerator regimes are separated by a boundary where $W = 0$ and $M(T_H) = M(T_C)$, which requires non-monotonic behaviour in $M(T)$, see Fig. 2(b)(iii).

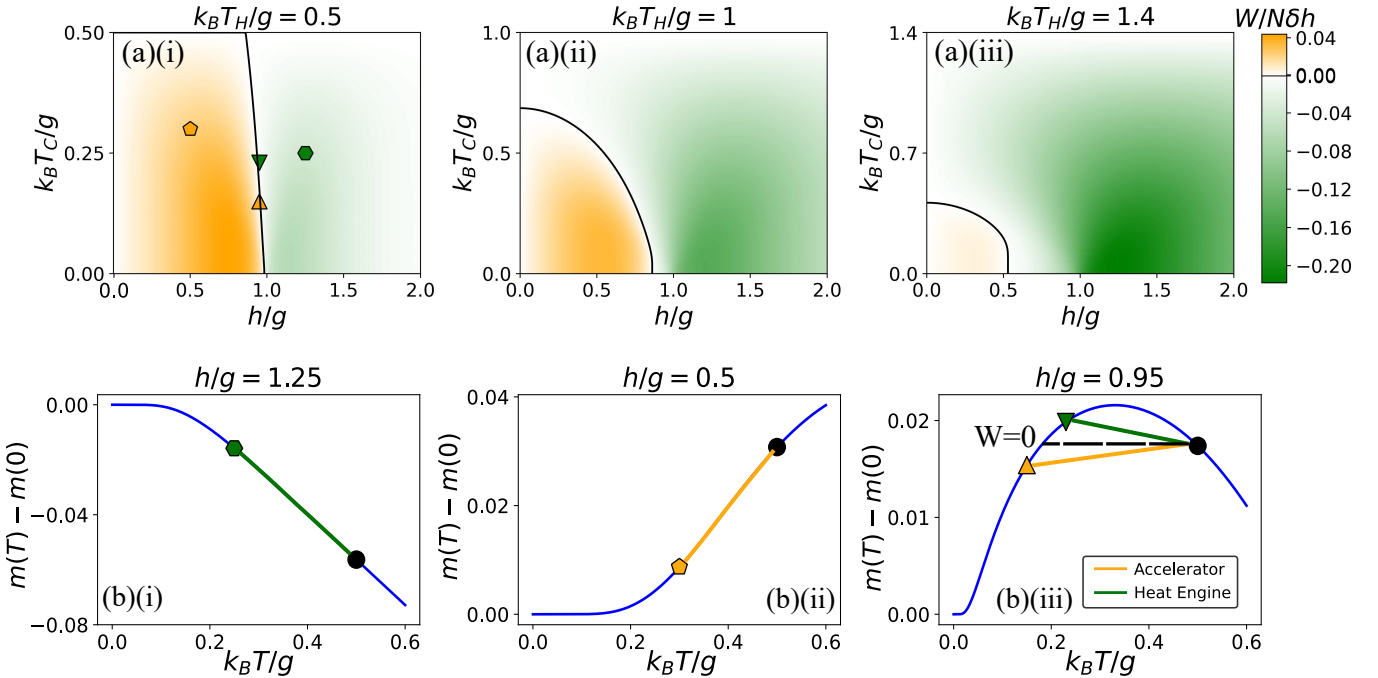


FIG. 2. (a) The engine (green) and accelerator (yellow) regimes for an Otto cycle with infinitesimal work stroke $\delta h = h_H - h_C > 0$ in the h - T_C plane. Panels (i)–(iii) correspond to $k_B T_H/g = 0.5$, $k_B T_H/g = 1$ and $k_B T_H/g = 1.4$, respectively. The size of work output ($W < 0$) or input ($W > 0$) is indicated by the colorbar. The black line represents the boundary between the engine and accelerator. (b) Transverse magnetization per particle $m(T) = M/N$ as a function of temperature for different h/g , with $m(0)$ the ground-state value. Black circles indicate $m(T_H)$ from (a)(i), whereas hexagon (i), pentagon (ii) and triangles (iii) indicate $m(T_C)$ corresponding to the four cycles marked in (a)(i). Engine operation occurs when $m(T_H) < m(T_C)$ whereas accelerator operation occurs when $m(T_H) > m(T_C)$. With the sign of δh fixed, a cross-over between the two regimes requires non-monotonic behaviour in $m(T)$, as shown in (iii).

1. $h > g$

For $h > g$, the magnetization decreases monotonically as the temperature increases, see Fig. 2(b,i) and Fig. 3. Hence $M(T_H) < M(T_C)$ and the system operates as an engine. This can be understood as follows. The ground state for $h > g$ is paramagnetic and hence will have maximum transverse magnetization. Excited levels resulting from spin-flips [37, 44] will have small transverse magnetization, and hence as these become occupied (T is increased), M will decrease. More precisely, using Eqs. (9), (10), we have

$$\frac{dM}{dT} = -\frac{4N}{\pi k_B T^2} \int_0^\pi d\theta (h - g \cos \theta) \operatorname{sech}^2 \left(\frac{\omega(\theta)}{2k_B T} \right). \quad (13)$$

For $h > g$ we have $dM/dT < 0$ for all T .

2. $h < g$ and low temperature

For $h < g$ the system can operate as an engine or an accelerator dependent on h and T . For sufficiently small h/g and low temperatures, the magnetization increases with temperature, see Fig. 2(b,ii) and Fig. 3. Hence

$M(T_H) > M(T_C)$ and the system operates as an accelerator. This behaviour can be understood from domain-wall quasiparticle excitations above the ferromagnetic ground state, which take the form [45],

$$|\psi_k\rangle = \frac{1}{\sqrt{N_k}} \sum_{n=1}^{N-1} \sin(n\theta_k) |n\rangle, \quad \theta_k = \frac{k\pi}{N}, k = 1, \dots, (N-1) \quad (14)$$

with energy $\mu(\theta) = 2(g - h \cos(\theta))$ [44]. Here N_k is the normalization factor and

$$|n\rangle = |\underbrace{-,-,\dots,-}_{1-n}, +, \dots, +\rangle \quad n = 1 \dots N-1, \quad (15)$$

are the $N-1$ degenerate lowest-energy domain-wall quasiparticle excitations for $h = 0$, where $|\pm\rangle = \frac{|0\rangle \pm |1\rangle}{\sqrt{2}}$ are the eigenstates of $\hat{\sigma}^x$. The transverse magnetization of the quasiparticle $|\psi_k\rangle$ arises from superpositions of states $|n\rangle$ and is given by

$$\begin{aligned} \langle \psi_k | \sum_j \hat{\sigma}_j^z | \psi_k \rangle &= \frac{2}{N_k} \sum_{n=1}^{N-1} \sin(n\theta_k) \sin((n+1)\theta_k) \\ &\approx \frac{1}{2}(N-1) \cos \theta_k. \end{aligned} \quad (16)$$

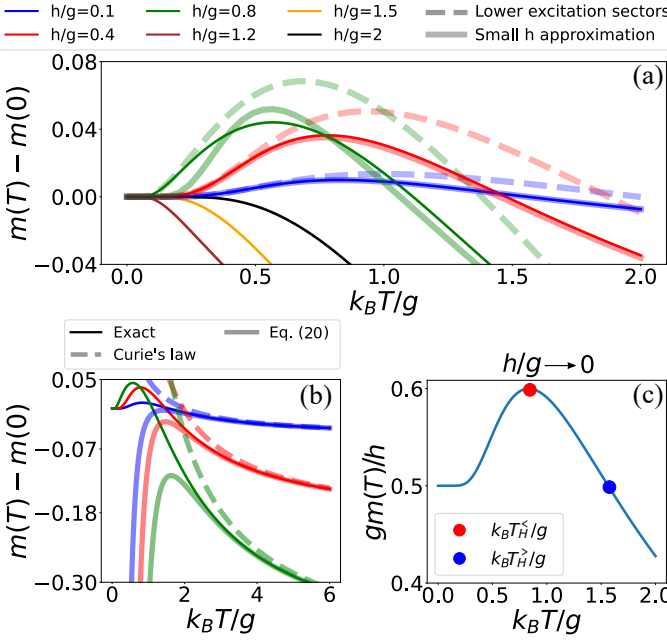


FIG. 3. (a) Variation of transverse magnetization per particle with temperature showing non-monotonic behaviour that gives rise to accelerator and engine operation. Dark, thin lines are the exact result and faint thicker lines are the small- h approximation Eq. (23). Dashed lines are the low-temperature approximation Eq. (22). (b) The transverse magnetization decreases with increasing temperature at high temperatures, resulting in engine operation. Colors correspond to values of h/g as in (a). Dark, thin lines are exact result and faint, thicker lines are the approximation Eq. (19). Dashed lines are Curie's law $m = h/k_B T$. (c) Transverse magnetization for small h/g , Eq. (20), highlighting the temperatures $T_H^<$ and $T_H^>$ (see text).

Hence the lower energy quasiparticles $0 < \theta < \pi/2$ are positively magnetized whereas the higher energy quasiparticles $\theta > \pi/2$ are negatively magnetized. Restricting the system to these quasiparticle excitations gives

$$F \approx -\frac{Nk_B T}{\pi} \int_0^\pi d\theta e^{-\frac{\mu(\theta)}{k_B T}}. \quad (17)$$

The net magnetization then satisfies

$$\frac{dM}{dT} \approx \frac{4N}{\pi k_B T^2} \int_0^\pi \mu(\theta) e^{-\frac{\mu(\theta)}{k_B T}} \cos(\theta) d\theta > 0, \quad (18)$$

at low temperatures, and hence results in accelerator operation.

3. High temperature regime

For high temperatures, $M(T)$ decreases monotonically with increasing temperature, see Fig. 3(a), and engine operation is observed, see Fig. 2(a). The high-temperature

behaviour of M can be obtained from Eq. (9) by expanding around $k_B T = \infty$, which gives

$$M = \frac{Nh}{k_B T} \left[1 - \frac{2g^2 + h^2}{3(k_B T)^2} + O\left(\frac{1}{(k_B T)^4}\right) \right]. \quad (19)$$

The dominant term in Eq. (19) follows Curie's law $M \propto h/k_B T$ and arises from high-temperature thermal fluctuations of the transverse spin. This results in engine operation and is present also in an ensemble of non-interacting spins. The effect of interactions on the magnetization appears at order $1/(k_B T)^3$ and requires correlations between the axial and transverse spin directions ($\partial^2 F / \partial h \partial g \neq 0$), which are suppressed at high temperatures. The result Eq. (19) predicts well the exact magnetization in the monotonic regime $k_B T \gtrsim 2g$, see Fig. 3(b).

4. Intermediate temperature regime

A cross-over between the accelerator and engine regime requires non-monotonic M and hence a peak where $dM/dT = 0$, see Fig. 2(b)(iii). This peak is only present for $h < g$, see Fig. 3(a), and separates the low and high temperature regimes described above. The crossover ($W = 0$ line) can be determined by solving $M(T_C) = M(T_H)$. To lowest order in h/g we have

$$M(T) = \frac{Nh}{2g} \left[\tanh\left(\frac{g}{k_B T}\right) + \frac{g}{k_B T} \operatorname{sech}^2\left(\frac{g}{k_B T}\right) \right], \quad (20)$$

which is plotted in Fig. 3(c). From this plot it is clear that $M(T_H) = M(T_C)$ has a non-trivial solution $T_H \neq T_C$ only for $T_H^< < T_H \leq T_H^>$. Here $k_B T_H^</g \approx 0.83$ is the temperature the magnetization peaks, obtained from Eq. (20) by solving $dM/dh = 0$. The higher temperature $k_B T_H^>/g = 1.56$ is obtained from Eq. (20) by solving $M(T) = M(0)$. For small h/g the system operates strictly as an accelerator for $T_H < T_H^<$ and as an engine for $T_H > T_H^>$.

With increasing h/g , the $W = 0$ boundary tends to move to lower T_C , see Fig. 2(a). For $h \rightarrow g$, the $W = 0$ point occurs at $T_C, T_H \rightarrow 0$. A change in sign of dM/dT requires a change in sign of $d\omega(\theta)/d\theta$ within the range of thermally accessible θ . We have $dM/dT = 0$ when

$$\frac{d\omega(\theta)}{dh} = \frac{2(h - g \cos \theta)}{\sqrt{g^2 + h^2 - 2gh \cos \theta}} \approx 0 \quad (21)$$

for some $\omega(\theta) \approx k_B T$. From this we can estimate that the $W = 0$ line occurs when $\omega(\theta)|_{h=g \cos \theta} = \sqrt{g^2 - h^2} \sim k_B T$, giving rise to a $W = 0$ line that moves to lower T_C as $k_B T_C \sim \sqrt{g^2 - h^2}$. Note the $W = 0$ boundary requires using a spectrum beyond the quasiparticle approximation, which has $dM/dT > 0$ always (Eq. (18)). Replacing $\mu(\theta)$ by $\omega(\theta)$ in Eq. (17) (equivalently expanding Eq. (9) in powers of $e^{-\omega(\theta)/k_B T}$) gives

$$M(T) = -\frac{4N}{\pi} \int_0^\pi d\theta \frac{h - g \cos(\theta)}{\omega(\theta)} e^{-\frac{\omega(\theta)}{k_B T}}. \quad (22)$$

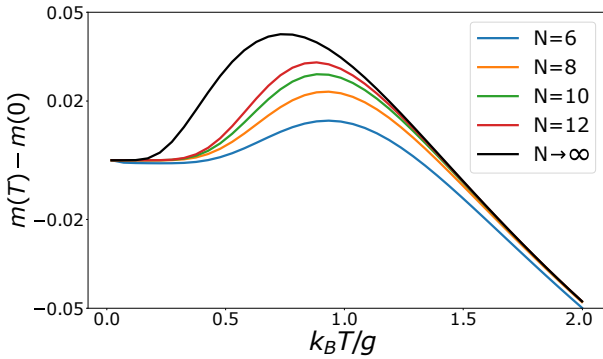


FIG. 4. The transverse magnetization per particle as a function of $k_B T/g$ for finite size systems with $h/g = 0.5$, compared to the thermodynamic limit. The curves are qualitatively similar and hence so are the regimes of thermal machine operation. Quantitatively $m(T) - m(0)$ decreases with N and the temperature range for which both accelerator and engine operation is possible (depending on the temperature of the cold reservoir) narrows.

The approximation Eq. (22) qualitatively predicts the peak in magnetization for $h < g$, see Fig. 3(a)

An accurate expression for M for $h < g$ can be obtained by expanding the full expression for M to third order in h/g . The resulting expression, however, is complicated,

$$M = \frac{Nh}{2g} (\tanh x + x \operatorname{sech}^2 x) - \frac{Nh^3}{16g^3} \left[6x^3 \operatorname{sech}^4 x - \tanh x + x \operatorname{sech}^2 x (1 - 4x^2 + 4x \tanh x) \right], \quad (23)$$

with $x = g/k_B T$. The approximation Eq. (23) agrees well with the exact magnetization for $h/g \lesssim 0.5$, see Fig. 3(a).

5. Finite-size effects

The magnetization for systems with a finite number of spins and $h < g$ are compared with the thermodynamic limit in Fig. 4. The finite-size system results are obtained using exact diagonalization with periodic boundary conditions, which gives closer agreement with the thermodynamic limit compared to open boundary conditions. The finite-size results are qualitatively the same as the thermodynamic limit, giving rise to strictly accelerator operation for sufficiently low temperatures of the hot bath and engine operation for sufficiently high temperatures [c.f. Fig. 3(c)]. Quantitatively $m(T) - m(0)$ decreases with decreasing N and hence the temperature range separating the strictly engine and accelerator regimes narrows as the system size is reduced, see Fig. 4. The decrease in $m(T) - m(0)$ with N occurs because the sparsely spaced energy levels in finite-size systems require a higher temperature to obtain a given transverse magnetization. We observe a cross-over to monotonically decreasing $m(T)$ for $h \approx g$, as for the thermodynamic limit, with the precise

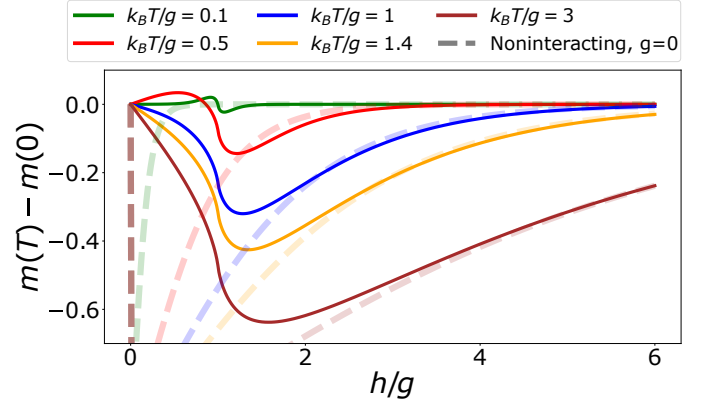


FIG. 5. The transverse magnetization per particle as a function of h/g . We can see $m(T) - m(0)$ exhibits a minimum near $h = g$ and therefore results in a maximum for $|W| = \delta h(m(T_H) - m(T_C))$, see Eq. (11). The magnetization approaches the non-interacting result Eq. (24) (dashed line) at large h/g ; in this regime $|W|$ decreases with increasing temperature.

cross-over sensitive to N . As h/g increases further the effect of interactions decreases and the finite-size results for $m(T)$ converge to the thermodynamic limit.

B. Magnitude of work output

We now briefly discuss the magnitude of work extracted (engine) or consumed (accelerator). In the high-temperature, low- h limit, $|W|$ increases with increasing h , see Fig. 2. This can be seen directly from the high temperature expansion Eq. (19), which also results in $|M(T_H) - M(T_C)|$ decreasing with increasing T for fixed T_H/T_C . In contrast, in the low-temperature, high- h limit, $|W|$ decreases with increasing h , see Fig. 2. When $h \gg g$, the transverse magnetization can be approximated by the magnetization of non-interacting spins,

$$M \approx N \tanh \left(\frac{h}{k_B T} \right), \quad (24)$$

For low temperatures $k_B T \ll h$ this gives $M \approx N(1 - 2e^{-h/k_B T})$, in which case we find $|M(T_H) - M(T_C)|$ increases with increasing T for fixed T_H/T_C . Both of these arguments also hold in the absence of interactions.

For $k_B T \lesssim g$, $|M(T) - M(0)|$ is largest around $h \approx g$, see Fig. 5. This results in a peak in $|W|$ for $h \approx g$, see Fig. 2. Such a peak has been discussed already in the low-temperature regime, in which case it can be explained in terms of a decreasing quasiparticle energy gap [16]. At low temperatures and for $h > g$, this results in a performance that exceeds that of non-interacting spins [16].

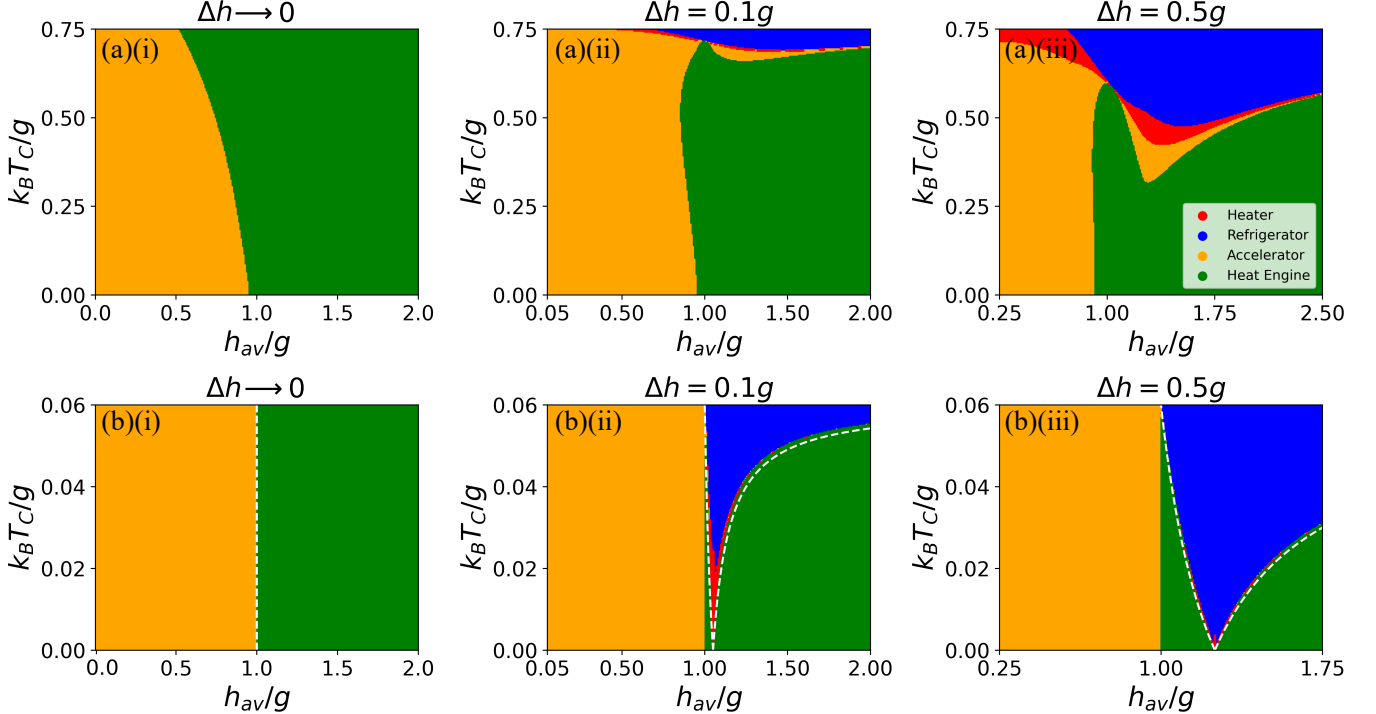


FIG. 6. (a) Thermal machine regions for increasing $\Delta h = h_H - h_C$, with (a) $k_B T_H/g = 0.75$ and (b) $k_B T_H/g = 0.06$. Finite-size Δh gives rise to heater and refrigerator regimes. White dashed lines in (b) represent the boundaries derived from the inequalities Eq. (27).

C. Finite-size work strokes

For an infinitesimal work stroke, the sign of the heat flows are fixed, restricting operation to either engine or accelerator, see Eq. (7). A finite-sized work stroke $\Delta h = h_H - h_C$ permits the thermal machine to operate as a refrigerator or a heater, see Fig. 6, where we have defined $h_{av} = (h_H + h_C)/2$.

To see how refrigeration operation may appear, it is simplest to first consider very low temperatures, in which case only the ground and first excited states have any significant thermal occupation [16]. The analysis then proceeds as for a single spin-1/2 system [42]. For low temperatures the heat flows are,

$$Q_H \approx 2|h_H - g| \left(e^{-|h_H - g|/k_B T_H} - e^{-|h_C - g|/k_B T_C} \right),$$

$$Q_C \approx 2|h_C - g| \left(e^{-|h_C - g|/k_B T_C} - e^{-|h_H - g|/k_B T_H} \right) \quad (25)$$

with $|h - g|$ the energy of the first excited level, which is the $k = 0$ quasiparticle excitation. From examination of Equation (25), it is clear that low-temperature refrigeration ($Q_H < 0, Q_C > 0$) occurs when

$$|h_H - g| > \frac{T_H}{T_C} |h_C - g|. \quad (26)$$

For $\Delta h > 0$ Eq. (26) is satisfied when

$$g + \frac{\Delta h T_H}{T_H + T_C} < h_H < g + \frac{\Delta h T_H}{T_H - T_C}. \quad (27)$$

The bounds of the inequality (27) accurately predict the low-temperature refrigerator boundary, see Fig. 6(b). Similar inequalities can be obtained from Eq. (26) for $\Delta h < 0$.

For higher temperatures, the analysis is qualitatively similar but complicated by the many levels present in the problem. This case has been discussed in recent works [21, 33, 36]. Notably, refrigerator operation is more effective when the temperature difference between T_H and T_C is small, and the influence of the critical point results in a peak in cooling capability [36]. Additionally, it was shown that as the size of the work stroke increases, the boundary of the refrigerator region expands to smaller T_C [33]. This expansion of the refrigerator region becomes more pronounced with work strokes across the critical point, as seen in Fig. 6.

All four regimes of operation appear for finite Δh at sufficiently high temperature, see Fig. 6(a). This gives rise to a “Carnot point” where $Q_H = Q_C = W = 0$ and all four regimes intersect [21, 42]. A sufficient condition for $Q_H = Q_C = W = 0$ is $r(\theta) = \omega_H(\theta)/\omega_C(\theta) = T_C/T_H$ for all θ [21]. The ratio r is insensitive to θ when $dr(\theta)/d\theta = 0$, which gives $g^2 = h_H h_C$ [using Eq. (3)]. Substituting this into r and setting $r = T_C/T_H$ gives values h_C^{cp} and h_H^{cp}

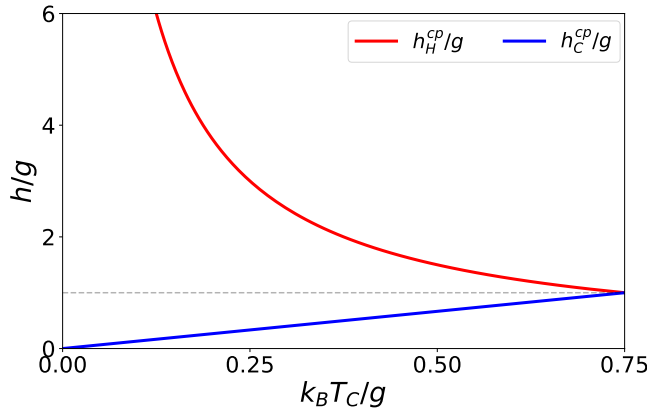


FIG. 7. Values of the driving h_H^{CP} and h_C^{CP} for a cycle with $Q_H = Q_C = W = 0$ [Eq. (28)], which gives rise to Carnot point where all four regimes of operation intersect, see Fig. 6(a)(ii) and (iii). We have $h_C^{\text{CP}} < g < h_H^{\text{CP}}$ and hence the work stroke necessarily crosses $h = g$ (horizontal dashed line). The temperature of the hot bath is fixed at $k_B T_H/g = 0.75$. We have also calculated h_C^{CP} and h_H^{CP} numerically using Eq. (5) and similar expressions for heat, which gives results indistinguishable from Eq. (28).

where $Q_H = Q_C = W = 0$ for given T_C , T_H and g [21],

$$h_C^{\text{CP}} = \frac{gT_C}{T_H}, \quad h_H^{\text{CP}} = \frac{gT_H}{T_C}. \quad (28)$$

The field strengths h_H^{CP} and h_C^{CP} are shown in Fig. 7. The Carnot point appears when Δh crosses g , since $h_C^{\text{CP}} < g < h_H^{\text{CP}}$. This is reasonable because the sign of $\frac{d\omega}{dh}$ is most sensitive to h near g , so small variations in h_{av} can lead to changes in the sign of W , Q_H and Q_C . For small Δh , the Carnot point will appear when $T_H \approx T_C$, as then only a small Δh is needed to change the flow of heat, see Fig. 6(a)(ii). As Δh increases ($h_H \gg g$), the accelerator and heater regimes shrink, and the system behavior converges to that of a noninteracting spin chain, where only the engine and refrigerator regimes remain.

When $k_B T_H - k_B T_C \gg |\Delta h|$ the sign of the heat flows are fixed and only accelerator or engine operation is possible. Furthermore, the $W = 0$ boundary separating these two regimes is unaffected by Δh at low temperatures, see Fig. 6. Focusing on just the ground and first excited state, as in Eq. (25), zero work output will occur when $|h_C - g| = |h_H - g|$, in which case the work stroke causes no net change in the energy of the first excited state. This gives $h_{\text{av}} = g$ irrespective of Δh .

IV. CONCLUSION

We have presented the quantum thermal machine regimes for the transverse-field Ising model with an infinitesimal work stroke. In this scenario the heat flows are fixed by the temperatures of the hot and cold reservoirs. This results in either the heat engine or accelerator

regime, dependent on the difference in equilibrium transverse magnetization at the two temperatures. We have identified the physical mechanisms behind the regimes of operation, connecting the low temperature operation to the behaviour of quasiparticles and the high temperature operation to an approximate equation of state for the system. This qualitative understanding also explains the regimes of operation for a finite-size work stroke when the difference in hot and cold reservoir temperatures are sufficiently large relative to the work stroke. Otherwise, refrigerator and heater regimes can emerge. Although most of our analysis here has been done in the thermodynamic limit, we have also shown that similar results hold in finite-size systems, as would be realised experimentally.

The realization of the transverse-field Ising model with either trapped ions or Rydberg atoms offers the potential to experimentally implement a many-body quantum thermal machine. Interactions between trapped ions are mediated by Coulomb forces, which can be modulated via optical dipole forces, and the transverse drive is an external magnetic field. Van der Waals forces mediate interactions between Rydberg atoms, and the transverse drive is a coherent laser. In both setups the work step can easily be implemented by varying the intensity of the transverse drive. Controlled heating and cooling of the system poses a challenge, but may be possible by applying external noise or light beams [46, 47]. The work done by the spins changes the power of the transverse drive, but the change is too small to be experimentally detectable [48]. The work done by the spins could instead be inferred from measuring the change in energy of the working substance itself [49] using site-resolved imaging [30, 50].

Our methodology and analysis will be useful in exploring other complex many-body quantum thermal machines, such as spin chains with long-range interactions and interacting Bose gases [7]. Diabatic work steps will likely modify the regimes of operation [42]. Considering infinitesimal work strokes would make diabatic operation amenable to a perturbative analysis [51] and allow counterdiabatic protocols to be incorporated [52], providing an interesting avenue for future research.

ACKNOWLEDGMENTS

This research was supported by The University of Queensland-IITD Academy of Research (UQIDAR), the Australian Research Council Centre of Excellence for Engineered Quantum Systems (CE170100009), and the Australian federal government Department of Industry, Science, and Resources via the Australia-India Strategic Research Fund (AIRXIV000025). We also acknowledge the support from the Indian Institute of Technology Delhi and SERB-DST, India.

[1] J. Millen and A. Xuereb, Perspective on quantum thermodynamics, *New J. Phys.* **18**, 011002 (2016).

[2] H. E. D. Scovil and E. O. Schulz-DuBois, Three-level masers as heat engines, *Phys. Rev. Lett.* **2**, 262 (1959).

[3] E. Geva and R. Kosloff, A quantum-mechanical heat engine operating in finite time. A model consisting of spin-1/2 systems as the working fluid, *J. Chem. Phys.* **96**, 3054 (1992).

[4] J. P. S. Peterson, T. B. Batalhão, M. Herrera, A. M. Souza, R. S. Sarthour, I. S. Oliveira, and R. M. Serra, Experimental characterization of a spin quantum heat engine, *Phys. Rev. Lett.* **123**, 240601 (2019).

[5] W. Niedenzu and G. Kurizki, Cooperative many-body enhancement of quantum thermal machine power, *New J. Phys.* **20**, 113038 (2018).

[6] V. Mukherjee and U. Divakaran, Many-body quantum thermal machines, *J. Phys.: Condens. Matter* **33**, 454001 (2021).

[7] L. M. Cangemi, C. Bhadra, and A. Levy, Quantum engines and refrigerators, *Phys. Rep.* **1087**, 1 (2024), quantum engines and refrigerators.

[8] R. Dillenschneider and E. Lutz, Energetics of quantum correlations, *EPL* **88**, 50003 (2009).

[9] O. Abah and E. Lutz, Efficiency of heat engines coupled to nonequilibrium reservoirs, *EPL* **106**, 20001 (2014).

[10] L. Williamson, F. Cerisola, J. Anders, and M. J. Davis, Extracting work from coherence in a two-mode Bose-Einstein condensate, [arXiv:2406.12410](https://arxiv.org/abs/2406.12410) (2024).

[11] J. Bengtsson, M. N. Tengstrand, A. Wacker, P. Samuelsson, M. Ueda, H. Linke, and S. M. Reimann, Quantum Szilard engine with attractively interacting bosons, *Phys. Rev. Lett.* **120**, 100601 (2018).

[12] Y.-Y. Chen, G. Watanabe, Y.-C. Yu, X.-W. Guan, and A. del Campo, An interaction-driven many-particle quantum heat engine and its universal behavior, *npj Quantum Inf.* **5**, 88 (2019).

[13] F. Carollo, F. M. Gambetta, K. Brandner, J. P. Garrahan, and I. Lesanovsky, Nonequilibrium quantum many-body Rydberg atom engine, *Phys. Rev. Lett.* **124**, 170602 (2020).

[14] T. Fogarty and T. Busch, A many-body heat engine at criticality, *Quantum Sci. Technol.* **6**, 015003 (2020).

[15] M. Boubakour, T. Fogarty, and T. Busch, Interaction-enhanced quantum heat engine, *Phys. Rev. Res.* **5**, 013088 (2023).

[16] L. A. Williamson and M. J. Davis, Many-body enhancement in a spin-chain quantum heat engine, *Phys. Rev. B* **109**, 024310 (2024).

[17] J. A. Estrada, F. Mayo, A. J. Roncaglia, and P. D. Mininni, Quantum engines with interacting Bose-Einstein condensates, *Phys. Rev. A* **109**, 012202 (2024).

[18] R. S. Watson and K. V. Kheruntsyan, Quantum many-body thermal machines enabled by atom-atom correlations, [arXiv:2308.05266v3](https://arxiv.org/abs/2308.05266v3) (2024).

[19] V. V. Nautiyal, R. S. Watson, and K. V. Kheruntsyan, A finite-time quantum Otto engine with tunnel coupled one-dimensional Bose gases, *New J. Phys.* **26**, 063033 (2024).

[20] N. Yunger Halpern, C. D. White, S. Gopalakrishnan, and G. Refael, Quantum engine based on many-body localization, *Phys. Rev. B* **99**, 024203 (2019).

[21] V. R. Arezzo, D. Rossini, and G. Piccitto, Many-body quantum heat engines based on free fermion systems, *Phys. Rev. B* **109**, 224309 (2024).

[22] P. Talkner, E. Lutz, and P. Hänggi, Fluctuation theorems: Work is not an observable, *Phys. Rev. E* **75**, 050102 (2007).

[23] H. T. Quan, Y.-x. Liu, C. P. Sun, and F. Nori, Quantum thermodynamic cycles and quantum heat engines, *Phys. Rev. E* **76**, 031105 (2007).

[24] F. Plastina, A. Aletti, T. J. G. Apollaro, G. Falcone, G. Francica, F. Galve, N. Lo Gullo, and R. Zambrini, Irreversible work and inner friction in quantum thermodynamic processes, *Phys. Rev. Lett.* **113**, 260601 (2014).

[25] D. Porras and J. I. Cirac, Effective quantum spin systems with trapped ions, *Phys. Rev. Lett.* **92**, 207901 (2004).

[26] J. W. Britton, B. C. Sawyer, A. C. Keith, C.-C. J. Wang, J. K. Freericks, H. Uys, M. J. Biercuk, and J. J. Bollinger, Engineered two-dimensional Ising interactions in a trapped-ion quantum simulator with hundreds of spins, *Nature* **484**, 489 (2012).

[27] J. G. Bohnet, B. C. Sawyer, J. W. Britton, M. L. Wall, A. M. Rey, M. Foss-Feig, and J. J. Bollinger, Quantum spin dynamics and entanglement generation with hundreds of trapped ions, *Science* **352**, 1297 (2016).

[28] J. Zhang, G. Pagano, P. W. Hess, A. Kyprianidis, P. Becker, H. Kaplan, A. V. Gorshkov, Z.-X. Gong, and C. Monroe, Observation of a many-body dynamical phase transition with a 53-qubit quantum simulator, *Nature* **551**, 601 (2017).

[29] C. Monroe, W. C. Campbell, L.-M. Duan, Z.-X. Gong, A. V. Gorshkov, P. W. Hess, R. Islam, K. Kim, N. M. Linke, G. Pagano, P. Richerme, C. Senko, and N. Y. Yao, Programmable quantum simulations of spin systems with trapped ions, *Rev. Mod. Phys.* **93**, 025001 (2021).

[30] H. Labuhn, D. Barredo, S. Ravets, S. de Léséleuc, T. Macrì, T. Lahaye, and A. Browaeys, Tunable two-dimensional arrays of single Rydberg atoms for realizing quantum Ising models, *Nature* **534**, 667 (2016).

[31] A. Browaeys and T. Lahaye, Many-body physics with individually controlled rydberg atoms, *Nat. Phys.* **16**, 132 (2020).

[32] M. Kloc, P. Cejnar, and G. Schaller, Collective performance of a finite-time quantum otto cycle, *Phys. Rev. E* **100**, 042126 (2019).

[33] G. Piccitto, M. Campisi, and D. Rossini, The Ising critical quantum Otto engine, *New J. Phys.* **24**, 103023 (2022).

[34] R. B. S. V. Mukherjee, U. Divakaran, and A. del Campo, Universal finite-time thermodynamics of many-body quantum machines from Kibble-Zurek scaling, *Phys. Rev. Res.* **2**, 043247 (2020).

[35] Q. Wang, Performance of quantum heat engines under the influence of long-range interactions, *Phys. Rev. E* **102**, 012138 (2020).

[36] A. Solfanelli, G. Giachetti, M. Campisi, S. Ruffo, and N. Defenu, Quantum heat engine with long-range advantages, *New J. Phys.* **25**, 033030 (2023).

[37] S. Sachdev, *Quantum Phase Transitions*, 2nd ed. (Cambridge University Press, 2011).

[38] P. Pfeuty, The one-dimensional Ising model with a transverse field, *Ann. Phys.* **57**, 79 (1970).

[39] R. Alicki, The quantum open system as a model of the

heat engine, *J. Phys. A.* **12**, L103 (1979).

[40] R. Kosloff, A quantum mechanical open system as a model of a heat engine, *J. Chem. Phys.* **80**, 1625 (1984).

[41] R. Kosloff and Y. Rezek, The quantum harmonic Otto cycle, *Entropy* **19** (2017).

[42] A. Solfanelli, M. Falsetti, and M. Campisi, Nonadiabatic single-qubit quantum Otto engine, *Phys. Rev. B* **101**, 054513 (2020).

[43] L. Fusco, S. Pigeon, T. J. G. Apollaro, A. Xuereb, L. Mazzola, M. Campisi, A. Ferraro, M. Paternostro, and G. De Chiara, Assessing the nonequilibrium thermodynamics in a quenched quantum many-body system via single projective measurements, *Phys. Rev. X* **4**, 031029 (2014).

[44] G. B. Mbeng, A. Russomanno, and G. E. Santoro, The quantum Ising chain for beginners, *SciPost Phys. Lect. Notes* , 82 (2024).

[45] We used open boundary condition while representing the states given by Eq. (14); the case with periodic boundary conditions will be similar, the only difference being that the domain walls come in pairs.

[46] J. Roßnagel, S. T. Dawkins, K. N. Tolazzi, O. Abah, E. Lutz, F. Schmidt-Kaler, and K. Singer, A single-atom heat engine, *Science* **352**, 325 (2016).

[47] Y. Zou, Y. Jiang, Y. Mei, X. Guo, and S. Du, Quantum heat engine using electromagnetically induced transparency, *Phys. Rev. Lett.* **119**, 050602 (2017).

[48] To see this, first note that adiabatic engine operation requires a cycle time $\lesssim h^{-1}$ and therefore the change in power P of the drive is $|\delta P| \lesssim h^2$. For a system driven by a magnetic field B we have $h = \mu B$, with μ the magnetic dipole moment of the spins, while for a system driven by an electric field E we have $h = dE$, with d the electric dipole moment. Estimating $\mu \sim \mu_B$ and $d \sim ea_B$, with μ_B the Bohr magneton, a_B the Bohr radius and e the electron charge, gives $|\delta P|/P \lesssim N\alpha^3 a_B^2/A$ for a magnetic drive and $|\delta P|/P \lesssim Naa_B^2/A$ for an electrical drive, with $\alpha = e^2/(4\pi\epsilon_0\hbar c)$ the fine structure constant and A the area of the drive. For an electric drive with a micron scale beam waist we have $|\delta P|/P \lesssim 10^{-11} N$; for a magnetic drive the output is even smaller.

[49] O. Onishchenko, G. Guarneri, P. Rosillo-Rodes, D. Pijn, J. Hilder, U. G. Poschinger, M. Perarnau-Llobet, J. Eisert, and F. Schmidt-Kaler, Probing coherent quantum thermodynamics using a trapped ion, *Nat. Commun.* **15**, 6974 (2024).

[50] R. Islam, E. E. Edwards, K. Kim, S. Korenblit, C. Noh, H. Carmichael, G.-D. Lin, L.-M. Duan, C.-C. Joseph Wang, J. K. Freericks, and C. Monroe, Onset of a quantum phase transition with a trapped ion quantum simulator, *Nat. Commun.* **2**, 377 (2011).

[51] M. Scandi, H. J. D. Miller, J. Anders, and M. Perarnau-Llobet, Quantum work statistics close to equilibrium, *Phys. Rev. Res.* **2**, 023377 (2020).

[52] A. del Campo, Shortcuts to adiabaticity by counterdiabatic driving, *Phys. Rev. Lett.* **111**, 100502 (2013).